Chemosphere 95 (2014) 50–57

Contents lists available at ScienceDirect

Chemosphere

journal homepage: www.elsevier.com/locate/chemosphere

Theoretical investigation on the mechanisms and kinetics of OH-initiated photooxidation of dimethyl phthalate (DMP) in atmosphere

Dandan Han [a], Jing Li [a], Haijie Cao [a], Maoxia He [a,*], Jingtian Hu [a], Side Yao [b]

[a] Environmental Research Institute, Shandong University, Jinan 250100, PR China
[b] Shanghai Institute of Applied Physics, Chinese Academy of Sciences, PO Box 800-204, Shanghai 201800, PR China

HIGHLIGHTS

- Quantum chemical methods are employed to study the title reactions.
- Major products of the title reactions are indicated in this study.
- The rate constant of title reaction is calculated in the first time.
- The lifetime of DMP is also determined.

ARTICLE INFO

Article history:
Received 27 March 2013
Received in revised form 22 July 2013
Accepted 30 July 2013
Available online 6 September 2013

Keywords:
Dimethy phthalate (DMP)
Hydroxylation reaction
Mechanism and kinetics
Rate constants

ABSTRACT

The atmospheric OH-initiated degradation mechanisms of dimethy phthalate (DMP) are analyzed at the MPWB1K/6-311++G(3df,2p)//MPWB1K/6-31+G(d,p) level of theory. The principal products detected experimentally are confirmed by this study while several major intermediates are reported for the first time. Additionally, the pathway scheme of hydroxylation reaction of DMP is proposed. The results about initial steps indicate that hydroxyl radical is most likely to be added to the *ortho*-carbon atom among additional reactions, while H atoms in methyl group are the most favorable to be abstracted by the OH radical. The rate constants of the elementary reactions over the temperature of 200–400 K were deduced using RRKM theory. The overall rate constant of the title reaction is 1.18×10^{-12} cm^3 molecule^{-1} s^{-1} at 298 K and 760 Torr while H abstraction reactions predominate. According to the rate constants given at different temperatures, the Arrhenius equation is fitted. The atmospheric half life of DMP with respect to OH is estimated to be 6.8 days.

1. Introduction

Phthalic acid esters (PAEs, also phthalate esters) are widely used in industrial applications. These compounds are mainly used in the soft polyvinyl chloride (PVC), adhesives and cellulose film coating (Vitali et al., 1997), and are possibly released into the environment throughout the entire service life and after the disposal of these materials (Staples et al., 1997). Thus, through inhalation, dermal contact and orally, humans are constantly exposed to phthalates. It has been found that the male reproductive system in some animals is adversely affected through the exposure to phthalates (Swan et al., 2005; Lottrup et al., 2006; Main et al., 2006). Also, the chronic aquatic toxicity data reviewed by Staples et al. (2011) indicates that C1—C4 PAEs are harmful to populations of fish and invertebrates. Moreover, several investigations have proven that some phthalates show weak estrogenic activity (Jobling et al., 1995; Harris et al., 1997).

Dimethyl phthalate (DMP), the simplest PAE, is common in environment because of its widespread usage and intractable biodegradability. DMP has been detected in the atmosphere, freshwaters, mineral waters, surface marine waters, and sediments (Staples et al., 2000; Teil et al., 2006; Montuori et al., 2008; Wang et al., 2008). As an endocrine-disrupting chemical, DMP can interfere with the reproductive systems of animals and humans and promote chromosome disorder in human leucocytes (Douglas et al., 1986; Allsopp et al., 1997; Staples et al., 1997). Also, DMP and its intermediates have been suspected to cause functional disturbances and nervous system abnormalities. Therefore, DMP has been listed as one of the priority pollutants by the US Environmental Protection Agency (USEPA) and other countries (US EPA, 1992; Wang et al., 1995). Hydrolysis, photodegradation and biodegradation are the removal types of DMP under different environmental conditions (Staples et al., 1997). However, for the degradation of

* Corresponding author. Tel.: +86 531 8836 1185; fax: +86 531 8836 1990.
E-mail address: hemaox@sdu.edu.cn (M. He).

0045-6535/$ - see front matter © 2013 Elsevier Ltd. All rights reserved.
http://dx.doi.org/10.1016/j.chemosphere.2013.07.087

DMP in the atmosphere, limited experimental investigations are reported and the actual reaction pathways are still unclear. By respiration and skin contact, the atmosphere DMP may accumulate in animals and lead to adverse effects. Therefore research on the removal of DMP from the atmosphere, which has been ignored in the past, should draw our attention in the future.

According to the previous study reviewed by Güsten et al. (1995) and Sabljić and Peijnenburg (2001), OH radical is the main oxidant in the atmosphere during daytime and is regarded as the air cleaner because of its ability to react with many kinds of pollutants in the atmosphere. Therefore, investigations into the OH initiated oxidation processes of pollutants are of major environmental interest.

With regard to DMP, although its atmospheric degradation cannot take place by direct photolysis, it can occur via indirect photolysis through reaction with OH radicals. The difficulty in experimental design and product monitoring leads to the lack of complete mechanism and detailed decomposition routes of DMP in atmosphere. Quantum chemical method has been successfully used in investigation on the environmental chemistry (Martell and Boyd, 1995; Sekušak et al., 1995; Sekušak et al., 1996). Also, Sekušak et al. (1997) and Sekušak and Sabljić (1997) have shown for the first time that hydrogen abstraction by OH radical proceeds by an indirect mechanism and the dual-level dynamic approach has been successfully used for the first time to calculate the reaction rate constants for such reactions. Thus, we employed the theoretical methods to obtain a detailed mechanistic and kinetic data on the photooxidation reaction of DMP, as a test compound.

The aim of this study is to understand the reaction mechanism thoroughly and to determine rate constants over a wide range of temperature for the reaction of OH with DMP using theoretical method. The reaction path profiles were constructed. Then the most favorable pathway was obtained. By the rate constants evaluation, the half lives of each compound as well as the branch ratios of various reaction channels were gained. We considered two reaction types between DMP and OH radicals, including OH-addition to aromatic ring and the abstractions of hydrogen from the aromatic ring and the methyl group.

2. Computational methods

2.1. Electronic structures

The Gaussian03 package was used for the quantum chemical calculations (Frisch et al., 2003). The geometrical optimizations of all stationary points were calculated by using the density functional theory MPWB1K method (Lynch et al., 2000) with 6-31+G(d,p) basis set. The convergence thresholds used for optimized structures are: maximum force, 4.5×10^{-4} au; rms force, 3.0×10^{-4} au; maximum displacement, 1.8×10^{-3} au; rms displacement, 1.2×10^{-3} au. The Cartesian coordinates are supplied in Table SM. Harmonic frequency calculations were carried out for the stationary points at the same level of theory to obtain activation energy (ΔE), reaction enthalpy (ΔH) and zero-point energies (ZPEs) to determine whether the optimized structures are minima or transition state. Intrinsic reaction coordinate (IRC) (Gonzalez and Schlegel, 1989) calculations were performed for each transition state to confirm that it is connected to the respective reactants and products. For the IRC calculations, stepsize = 2 amu$^{1/2}$ Bohr, maxpoints = 100 and maxcyc = 40. The single point energies of optimized structures were obtained with the level of MPWB1K/6-311++G(3df,2p) to improve the quality of barrier heights. The reaction path profiles were constructed at the MPWB1K/6-311++G(3df,2p)//MPWB1K/6-31+G(d,p) level of theory.

2.2. Rate constants

Energy-grained master equation calculations (Miller and Klippenstein, 2006) were executed to investigate the statistical mechanics of the title reaction. All master-equation (ME) calculations are performed using the program MESMER (Robertson et al., 2008). The form of master equation used in this work is

$$\frac{dp}{dt} = Mp \tag{1}$$

where p is the population distribution vector and M is a collision/reaction matrix that describes collisional energy transfer between the states and reaction from the energized states.

The microcanonical rate coefficient $k(E)$ for each elementary reaction in this paper follows the equation:

$$k(E) = \frac{W(E)}{h\rho(E)} \tag{2}$$

Here $W(E)$ is the sum of rovibrational states at the optimized transition state geometry and $\rho(E)$ is the density of rovibrational states of the reactant.

When using MESMER for bimolecular reactions, the main restriction being that one of the reactants must be in excess, so that the bimolecular association occurs under pseudo-first order conditions. A generic association reaction A + B $\rightleftharpoons$ C has a forward association rate constant, k_a, and a backward dissociation rate constant, k_d. If the conditions are such that [A] $\gg$ [B], this reaction can be represented as pseudo-isomerization reaction, where the forward rate coefficient is $k'_a = k_a$ [A]. The concentration of OH radical is in excess in our work, so that all 12 elementary reactions (R1)–(R6), (R1b), (R2b), (R3b), (R4b), (R5b), (R6b) studied in this paper should be considered pseudo-first order conditions. Thus, RRKM theory could be applied in this method.

The pressure range in the calculation is 100–1500 Torr provided with helium, of which the molecular weight is 4.0 and Lennard–Jones parameters are $\sigma = 2.55$ and $\varepsilon = 10.2$. The grain size is 100 cm^{-1} and the maximum grain energy is 258 kT for the calculation of rate constants. Classical method was used for calculating density of states. Simple RRKM method was used for the calculation of microcanonical rate coefficients of (R1)-(R5), (R1b), (R2b), (R3b), (R4b), (R5b), while MesmerILT method was provided for (R6) and (R6b). The exponential down model was implemented for describing collisional transfer probabilities in this calculation. The calculation of the quantum mechanical energy levels of a hindered rotation is based on a one dimensional rotational eigenfunctions. Eckart coefficient approximates tunneling using a one dimensional asymmetric Eckart potential. The precision used for calculation is double.

3. Results and discussion

3.1. Mechanism of reactions

Two energy minima of DMP are considered, and the structures of them are depicted in Schemes 1 and 2. The sum of electronic and zero-point energies (E_0) and sum of electronic and thermal free energies (G) for Structures 1 and 2 of DMP are −687.52, −687.50 and −687.56, −687.54 Hartree/Particle, respectively.

Comparing the thermodynamic parameters shown above, Structure 1 is more stable than the other one. Therefore, we choose the first structure for our calculations in this work. The total possible reaction channels are shown in Figs. 1–3. The schematic energetic profiles of PESs are plotted in Figs. 4–6. The geometrical structures of all stationary points including reactants, intermediates, transition states and products relative to the title reactions are depicted in Fig. SM(a, b) in Supplementary Material.

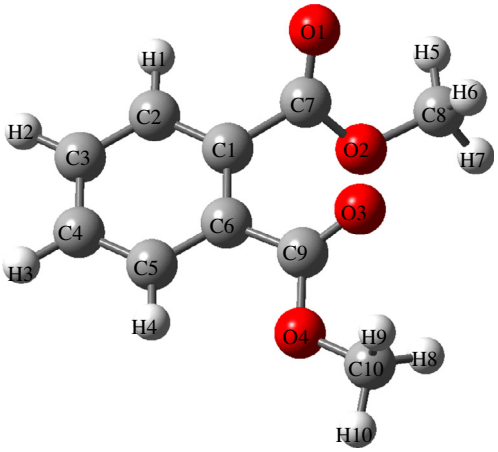

Scheme 1. Structure 1 of DMP.

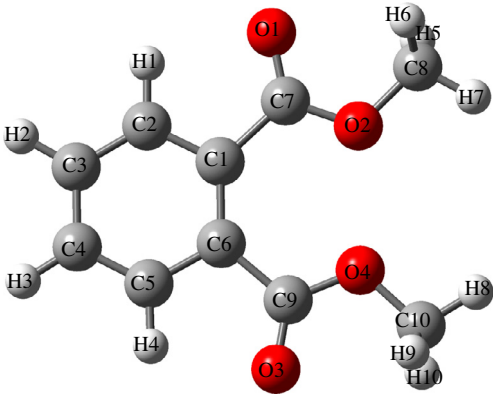

Scheme 2. Structure 2 of DMP.

3.1.1. Initial reaction of DMP with OH radicals

As shown in Fig. 1, the attack of OH radical to DMP can be classified as two types: OH-addition to phenyl ring and H-abstraction from the phenyl ring and the eater methyl groups.

With regard to the OH-addition reactions, six sites in the phenyl ring of DMP are considered. As for the H-abstraction reactions, there are also six positions taken into account. All these initial reactions proceed via the generation of the pre-reaction complexes. The primary reaction channels are presented as follows:

$$\mathrm{DMP + OH \rightarrow IM01 \rightarrow\ TS1 \rightarrow IM1}\quad \text{OH-addition to } C_1 \text{ atom} \tag{R1}$$

$$\rightarrow \mathrm{IM02 \rightarrow TS2 \rightarrow IM2}\quad \text{OH-addition to } C_2 \text{ atom} \tag{R2}$$

$$\rightarrow \mathrm{IM03 \rightarrow TS3 \rightarrow IM3}\quad \text{OH-addition to } C_3 \text{ atom} \tag{R3}$$

$$\rightarrow \mathrm{IM04 \rightarrow TS4 \rightarrow IM4 + H_2O}\quad \text{H abstraction from } C_2\text{—H of phenyl ring} \tag{R4}$$

$$\rightarrow \mathrm{IM05 \rightarrow TS5 \rightarrow IM5 + H_2O}\quad \text{H abstraction from} C_3\text{—H of phenyl ring} \tag{R5}$$

$$\rightarrow \mathrm{IM06 \rightarrow TS6 \rightarrow IM6 + H_2O}\quad \text{H abstraction from } CH_3 \text{ group-C8} \tag{R6}$$

$$\rightarrow \mathrm{IM01b \rightarrow TS1b \rightarrow IM1b}\quad \text{OH-addition to } C_6 \text{ atom} \tag{R1b}$$

$$\rightarrow \mathrm{IM02b \rightarrow TS2b \rightarrow IM2b}\quad \text{OH-addition to } C_5 \text{ atom} \tag{R2b}$$

$$\rightarrow \mathrm{IM03b \rightarrow TS3b \rightarrow IM3b}\quad \text{OH-addition to } C_4 \text{ atom} \tag{R3b}$$

$$\rightarrow \mathrm{IM04b \rightarrow TS4b \rightarrow IM4b + H_2O}\quad \text{H abstraction from } C_5\text{—H of phenyl ring} \tag{R4b}$$

$$\rightarrow \mathrm{IM05b \rightarrow TS5b \rightarrow IM5b + H_2O}\quad \text{H abstraction from } C_4\text{—H of phenyl ring} \tag{R5b}$$

$$\rightarrow \mathrm{IM06b \rightarrow TS6b \rightarrow IM6b + H_2O}\quad \text{H abstraction from } CH_3 \text{ group-C10} \tag{R6b}$$

The zero-point corrected reaction enthalpies of these channels are given in Fig. 1. For the addition processes, the attacking of OH to the carbon atom in aromatic ring primarily generates the pre-reaction complexes. Similar to the reactions between OH and fluorobenzene or chlorobenzene (Kovacevic and Sabljic, 2013a,b), the pre-reaction complexes during the OH-addition reaction are stable structures. Among the additional processes, the OH radical attacking to the ortho-carbon processes ((R2) and (R2b)) possess the lowest energy barrier and high exothermic heat making them the most favorable reactions. Meanwhile, the H-abstraction reactions would occur in the branched chains ((R6) and (R6b)) rather than the phenyl ring. Considering the similarity between the Reactions (R2) and (R2b), we select (R2) for the further discussion, and (R6) is also chosen due to the same reason. The detailed description of (R2) and (R6) will be revealed in the following section.

OH radical attacking to the C2 atom primarily generates a van der Waals complex IM02, in which a H-bonding exists with the length of H11—O1 is 1.894 Å. IM02 possesses 21.2 kJ mol^{-1} energy lower than the reactants. Subsequently, the primary adduct (IM2) formed via the transition state TS2, which lies 29.8 kJ mol^{-1} above IM02. In IM2 and TS2, the H-bonding still exists with the lengths of 2.042 and 2.137 Å. The bond lengths of C2—O5 (1.926 Å in TS2 and 1.410 Å in IM2) are shortened by 1.243 and 1.759 Å compared with that in IM02. Also the obvious approaching tendency between C2 and O5 is clearly shown by IRC calculation. With the addition of the high exothermic heat (73.2 kJ mol^{-1}), this process can occur readily. The further reaction of IM2 is unavoidable because the cyclohexadienyl radical is an unstable structure.

For the Reaction (R6), the pre-reaction complex IM06, with the stabilization energy of −20.2 kJ mol^{-1}, is firstly generated through the approaching of OH to the atom H5. The bond lengths of H5—O5 and H11—O1 are 2.780 and 1.884 Å, respectively. And then, the H atom is abstracted by OH radical via the transition state TS6, leading to the primary adduct IM6 and H_2O, which lies 74.9 kJ mol^{-1} below reactants. The bond lengths of C8—H5 and O5—H5 in TS6 are 1.213 Å and 1.291 Å, which are 0.128 Å and 0.338 Å longer than that in reactant adduct and H_2O. The IRC calculation also testifies the simultaneous tendency of the rupture of C8—H5 and the formation of O5—H5. Due to the abundant existence of NO and O_2, etc., the following reaction of IM6 with these molecules will undergo inevitably.

3.1.2. Secondary reaction

IM2 and IM6, as the major primary products according to the above discussion, are taken into account in this section.

Considering the possible active positions and the directions of O_2 attacking to the phenyl ring (the same direction or opposite direction with OH), there are five patterns for the reaction of IM2 + O_2, shown in Fig. 2. Here, we define the same direction with OH as "**a**" model, while the opposite direction with OH as "**b**" model.

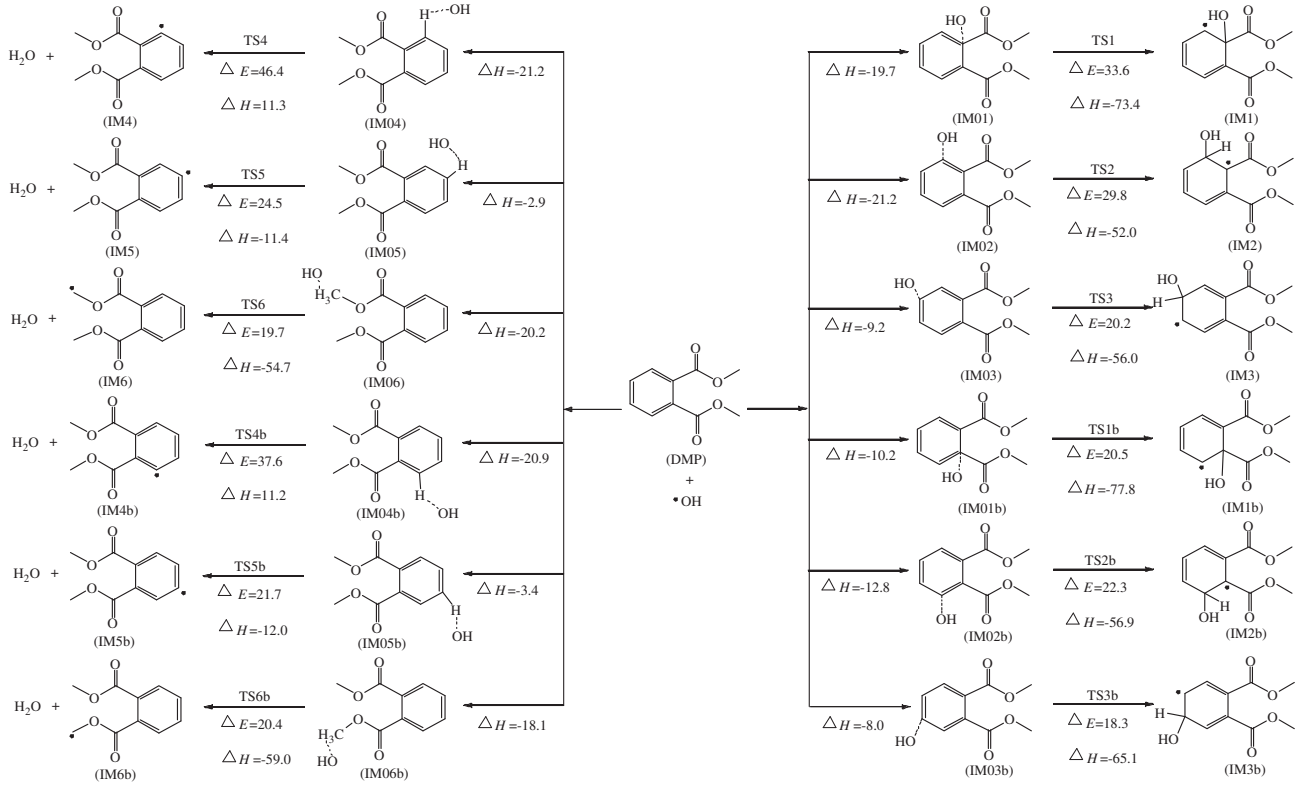

Fig. 1. The primary reaction paths of DMP with OH at the MPWB1K/6-31+G(d,p) level of theory: energy barriers ΔE (kJ mol^{-1}) and reaction enthalpy ΔH (kJ mol^{-1}) are calculated at 298 K.

Because of the steric-hindrance effect brought about by OH radical, it is scarcely possible for the approaching of O_2 molecule to C1 atom with "**a**" model. C1 atom is firstly attached by O_2 with "**b**" model via TS2-1b, which results in the formation of IM2-1b with the low barrier of 48.6 kJ mol^{-1} and exothermic heat of 8.7 kJ mol^{-1}. A new bond between C1 and O6 of O_2 is formed with the bond length of C1—O6 in IM2-1b is 1.464 Å, which is 0.514 Å shorter than that in TS2-1b. For C3 reaction site, two reaction patterns are considered. One is the production of IM2-3a, accompanied by the transition state TS2-3a, which lies at 60.1 kJ mol^{-1} of energy higher than IM2 + O_2. The 14.3 kJ mol^{-1} of energy is released in this process. The other pathway is the approaching of O_2 to C3 atom via TS2-3b, which generates IM2-3b. The barrier energy and exothermic heat of this channel are 55.0 and 21.6 kJ mol^{-1}, respectively. Both bond distances of C3—O6 in IM2-3a and IM2-3b are 1.446 Å, which are respectively shortened by 28.1% and 27.4% comparing with that in TS2-3a and TS2-3b. Although the value of barrier energy and exothermic heat of the two channels are similar, the production of IM2-3b is slightly superior to IM2-3a. This conclusion should be attributed to the steric-hindrance effect of OH radical attached in the IM2. With regard to the reaction position C5, two models, resulting in IM2-5a and IM2-5b respectively via TS2-5a and TS2-5b, are adopted during the reaction process. The corresponding exothermic energies and barrier heats of these two pathways are 8.8, 9.6 and 56.1, 45.5 kJ mol^{-1}, respectively. The bond lengths of the new formed bond C5—O6 (1.454 Å in IM2-5a and 1.474 Å in IM2-5b) are shortened about 25.8% relative to that in TS2-5a and TS2-5b. Also owing to the existence of OH, the formation of IM2-5b is much easier than IM2-5a. Comparing with the energy barriers and exothermic heats of the above five patterns, we can infer that the most favorable reaction channels are IM2 + O_2 → TS2-1b → IM2-1b and IM2 + O_2 → TS2-5b → IM2-5b. Furthermore, subsequent rearrangement reactions will occur readily owing to the instability of IM2-1b and IM2-5b.

For IM2-1b, the O7 atom possesses free electrons and it will attach to the active sites (C3/C5) in the phenyl ring, forming the five-numbered ring (C1—O6—O7—C3—C2/C1—O6—O7—C5—C6). The formation of IM2-1b-a is an exothermic reaction with 63.1 kJ mol^{-1} heat released, while the generation of IM2-1b-b is endothermic pathway with the absorption of 0.6 kJ mol^{-1} heat. As well as that, the energy barriers of the two channels are 44.1 kJ mol^{-1} and 115.0 kJ mol^{-1}. Hence, we can say that the process of the generation of IM2-1b-a is more likely to occur than IM2-1b-b. The bond lengths of C3—O7 and C5—O7 in the cyclization products IM2-1b-a (1.419 Å) and IM2-1b-b (1.419 Å) are 0.552 and 0.589 Å shorter than that in TS2-1b-a and TS2-1b-b, respectively. Similar to the IM2-1b, IM2-5b will subsequently carry out the cyclization reaction, resulting in the five-numbered rings IM2-5b-a and IM2-5b-b via TS2-5b-a and TS2-5b-b (Fig. SM), respectively. The energy barriers of the two reactions are 114.8 and 132.4 kJ mol^{-1}, and those are endothermic processes with the absorption heat of 1.5 and 25.5 kJ mol^{-1}. In comparison with the corresponding value of the cyclization reaction of IM2-1b, both self-cyclization reactions of IM2-5b are obviously unlikely to occur. Therefore, we select IM2-1b for the further calculation to decrease the cost of computation.

According to the conclusion we have obtained above, the formation of IM2-1b-a is thermodynamically favorable pathway for the cyclization reaction of IM2-1b. IM2-1b-a is not a stable product because of the active site (C4) in the phenyl ring, and it will react with another O_2 in the following step. As shown in Fig. 3, the second O_2 molecular attacks C4 atom in IM2-1b-a from the opposite site of the first O_2, with the O9 atom oriented towards the center of phenyl ring. The transition state of this process is TS2-1b-a1, in which the bond distance of C4—O8 is 1.983 Å. The relative bond length in the adduct IM2-1b-a1 is 0.544 Å shorter than that in TS2-1b-3-O_2.

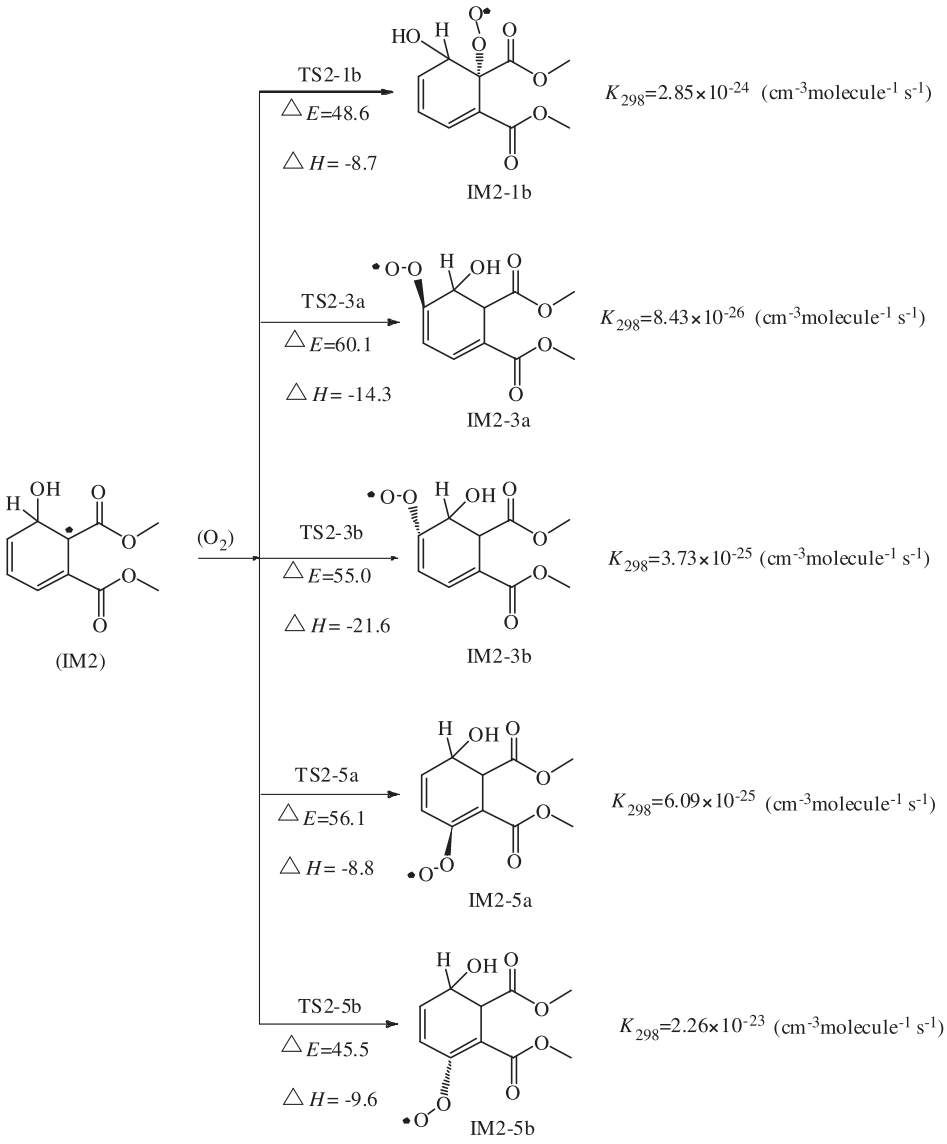

Fig. 2. The further reaction paths of IM2 at the MPWB1K/6-31+G(d,p) level of theory and the corresponding rate constants at 298 K: energy barriers ΔE (kJ mol^{-1}) and reaction enthalpy ΔH (kJ mol^{-1}) are calculated at 298 K.

This process has the energy barrier of 64.4 kJ mol^{-1} and exothermic heat of 40.2 kJ mol^{-1}. The active intermediate IM2-1b-a1 then combines the dissociative NO molecule via a barrier-free process to produce IM2-1b-a2. This favorable pathway is exothermic by 69.3 kJ mol^{-1}. The following reaction is the formation of oxyl radical IM2-1b-a3 and NO_2 or the elimination of HNO_2 to form the final product P2-1b-1. The first channel is carried out via the transition state TS2-1b-a3 with the energy barrier of 143.4 kJ mol^{-1} and exothermic heat of 2.3 kJ mol^{-1}, while the later one should overcome 112.7 kJ mol^{-1} energy and release much greater energy of 216.1 kJ mol^{-1}. Therefore, the later one is of critical importance in the dissociation process of IM2-1b-a1 and thus P2-1b-1 may be the dominant product in the whole reaction. For the cycloreversion reaction of IM2-1b-a3, there are two pathways. One mode is the generation of the double bond C4═O8 and the cleavage of C3—C4 via transition state TS2-1b-a5, which occur simultaneously and result in IM2-1b-a5. The energy barrier and the endothermic energy of this process are 58.7 and 18.0 kJ mol^{-1}, respectively. The other mode is the formation of C4═O8 double bond and the rupture of C4—C5 bond to produce IM2-1b-a4, with the transition state TS2-1b-a4. Because of the high-energy barrier (121.8 kJ mol^{-1}) and the high-endothermic heat (109.9 kJ mol^{-1}) compared to the corresponding value of the first mode, the latter one will hardly occur. Therefore, the major product of this cycloreversion reaction is IM2-1b-a5. Subsequently, IM2-1b-a6 is formed via the cleavage of O6═O7 and the formation of C3═O7 bond in IM2-1b-a5, which is a barrier-free reaction with a high exothermic heat of 183.1 kJ mol^{-1}.

For IM2-1b-a6, three self-decomposition patterns are taken into account. First, the breaking of C1—C2 bond and the generation of C1═O6 double bond in IM2-1b-a6 could take place simultaneously. via the transition state TS2-1b-a6, the final product P2-1b-2 and intermediate IM2-1b-a7 are formed. In this process, only 2.0 kJ mol^{-1} energy barrier should be overcome, and the released heat quantity is 45.6 kJ mol^{-1}. Then, IM2-1b-a7 break down to P2-1b-3 and H radical is released via the transition state TS2-1b-a9, respectively with the energy barrier and endothermic heat of 96.9 and 0.3 kJ mol^{-1}. Second, the self-dissociation is carried out by the concerted rupture of C1—C7 bond and generation of C1═O6 bond in IM2-1b-a6 via the transition state TS2-1b-a7. The production of P2-1b-4 + IM2-1b-a8 is an endothermic process, with the absorption heat of 39.1 kJ mol^{-1} and energy barrier of 48.6 kJ mol^{-1}. For the last pattern, it should overcome the energy barrier of 97.3 kJ mol^{-1} and absorb 73.8 kJ mol^{-1} heat quantities

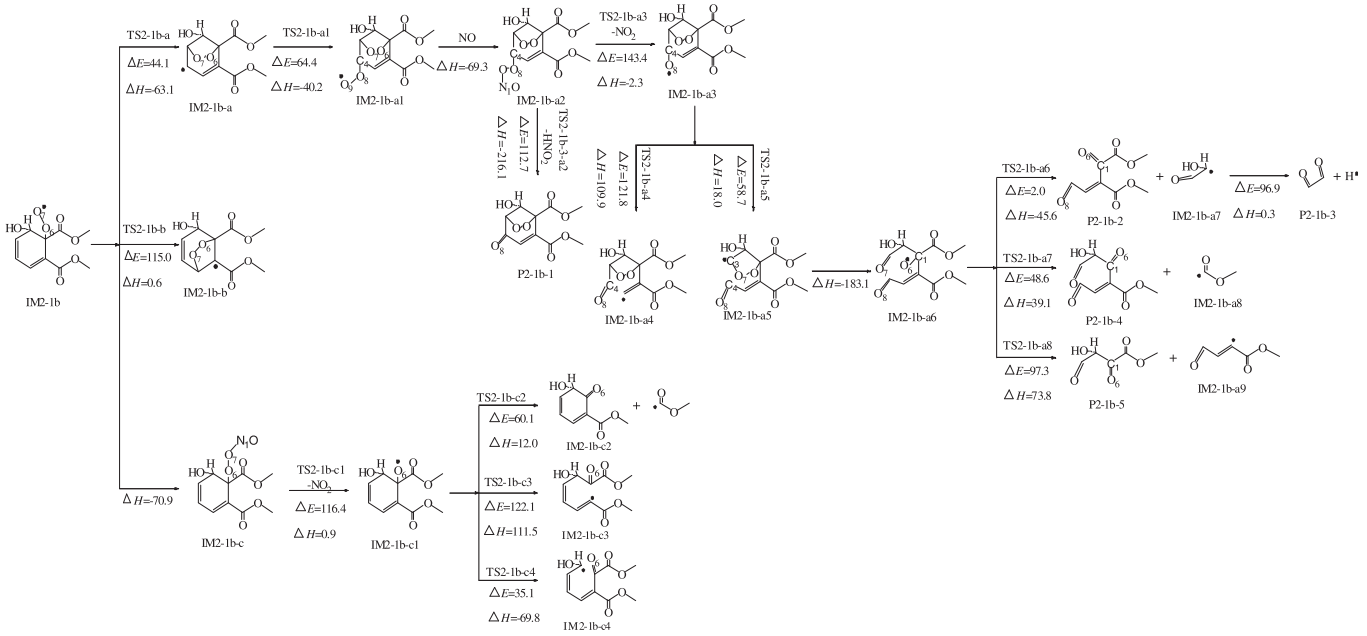

Fig. 3. The further reaction paths of IM2-1b at the MPWB1K/6-31+G(d,p) level of theory: energy barriers ΔE (kJ mol^{-1}) and reaction enthalpy ΔH (kJ mol^{-1}) are calculated at 298 K.

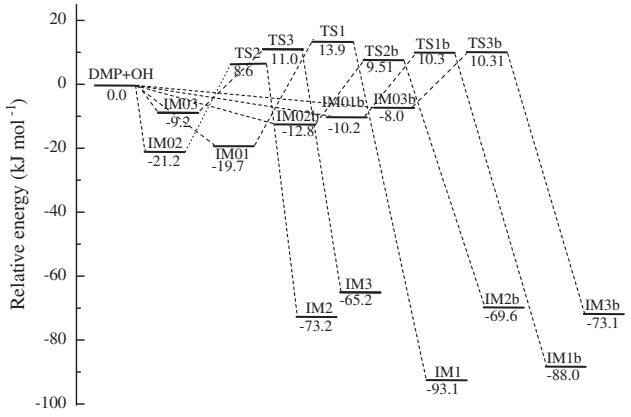

Fig. 4. Profiles of the potential energy surface for the primary addition reaction of DMP + OH.

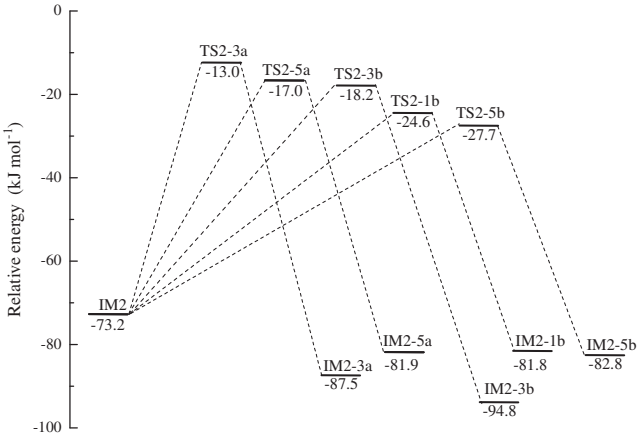

Fig. 6. The reaction path profiles for the further reaction of IM2.

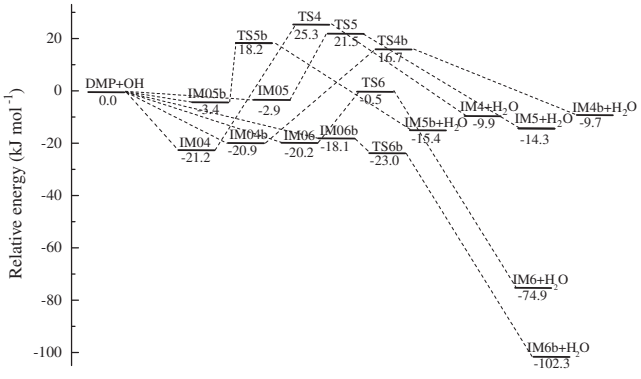

Fig. 5. The reaction path profiles of the primary H-abstraction reaction of DMP + OH.

to form P2-1b-5 + IM2-1b-a9 via the transition state TS2-1b-a8. The high-energy barrier and high endothermicity certify that this pathway is unlikely to occur. Based on the above analysis, the major products of the self-cyclization reaction of IM2-1b are IM2-1b-a2, P2-1b-1, and P2-1b-3 (oxalaldehyde), while the minor products are several poly-ketone compounds.

IM2-1b could also react in the troposphere with the NO molecule. The formation of O7—N1 bond in IM2-1b-c is a barrier-free process with an exothermic energy of 70.9 kJ mol^{-1} and results in IM2-1b-C. The elimination of NO_2 in the following step generates an intermediate IM2-1b-c1 with the high-energy barrier of 116.4 kJ mol^{-1} and endothermic energy of 0.9 kJ mol^{-1}. Three reaction modes are possible for the subsequent self-dissociation of IM2-1b-c1. The formation of C1═O6 double bond in IM2-1b-c1 can coincide with the rupture of C1—C7/C1—C2/C1—C6 bonds, resulting in the formation of IM2-1b-c2/IM2-1b-c3/IM2-1b-c4. The energy barriers and the reaction enthalpies of these three channels are respectively 60.1, 122.1, 35.1 kJ mol^{-1} and 12.0, 111.5, −69.8 kJ mol^{-1}. Consequently, the third reaction is the most thermodynamically favorable channel. According to the description above, the dominant product of the reaction of IM2-1b + NO is IM2-1b-c4.

Table 1
The individual rate constants (cm^{-3} $molecule^{-1}$ s^{-1}) of the primary reaction of DMP + OH at different temperatures (K).

	200 K	250 K	298 K	325 K	350 K	375 K	400 K	Equation
k_{R1}	7.06E−41	7.18E−17	5.32E−17	4.32E−16	5.00E−16	7.01E−16	9.29E−16	1.20×10^{11} exp(−20,711/T)
k_{R1b}	3.86E−38	2.72E−36	1.98E−15	3.93E−15	5.24E−15	6.72E−15	8.44E−15	8.48×10^{16} exp(−25,828/T)
k_{R2}	4.80E−16	1.93E−15	2.63E−15	3.55E−15	4.49E−15	5.55E−15	6.60E−15	8.02×10^{-14} exp(−999/T)
k_{R2b}	4.85E−16	1.36E−15	2.57E−15	3.30E−15	4.00E−15	4.25E−15	4.75E−15	5.35×10^{-14} exp(−927/T)
k_{R3}	1.94E−16	7.05E−16	1.68E−15	2.29E−15	2.92E−15	3.52E−15	4.08E−15	9.74×10^{-14} exp(−1234/T)
k_{R3b}	3.18E−16	8.80E−16	1.92E−15	2.29E−15	2.84E−15	3.02E−15	3.44E−15	4.32×10^{-14} exp(−971/T)
k_{R4}	3.60E−20	5.36E−19	1.85E−18	2.56E−18	2.99E−18	3.18E−18	3.19E−18	5.14×10^{-16} exp(−1819/T)
k_{R4b}	2.57E−18	6.10E−18	6.50E−18	5.89E−18	5.17E−18	4.45E−18	3.79E−18	7.89×10^{-18} exp(−153/T)
k_{R5}	5.74E−19	3.12E−18	4.82E−18	4.75E−18	4.30E−18	3.72E−18	3.14E−18	2.96×10^{-17} exp(−686/T)
k_{R5b}	5.70E−19	3.94E−18	7.25E−18	7.59E−18	7.14E−18	6.34E−18	5.44E−18	9.38×10^{-17} exp(−915/T)
k_{R6}	1.22E−12	6.89E−13	6.51E−13	6.04E−13	5.35E−13	4.45E−13	3.44E−13	1.42×10^{-13} exp(428/T)
k_{R6b}	7.02E−13	6.55E−13	5.19E−13	4.04E−13	2.93E−13	1.97E−13	1.25E−13	4.45×10^{-14} exp(619/T)

IM6 (Fig. SM) will further react with O_2 with the exothermic heat quantities of 200.8 kJ mol^{-1}, which is followed by the formation of IM6—NO with 64.7 kJ mol^{-1} energies released. Subsequently, the elimination of HNO_2 occurs via transition state TS6-HNO2, leading to the formation of IM6-HNO2. The energy barrier and exothermic energy of this process are 111.3 and 220.9 kJ mol^{-1}, with the major product IM6-HNO2.

In total the final products of the title reaction are IM6-HNO2, oxalaldehyde and several poly-ketone compounds. Due to the lack of complementary experimental studies about the atmospheric reaction between DMP and OH radicals, the mechanism mentioned in this study may be the guidance for future experimental studies.

3.2. Kinetic properties

Rate constants of the primary reaction channels are calculated over the temperature range of 200–400 K and the pressure range of 100–1500 Torr, and the corresponding Arrhenius equations under 760 Torr are listed in Table 1. With the comparison of individual rate coefficients of DMP + OH (Table 1), the most favorable channels are (R2) (OH-addition reaction) and (R6) (H-abstraction reaction). This conclusion is in line with the result inferred from the thermodynamic data. According to the room temperature rate constants of the reaction IM2 + O_2 (Fig. 2), we can indicate that O_2 attacking to C1 and C5 are the main pathways among all the channels.

To clarify the major reaction mode in this study, the overall rate coefficient of H-abstraction reactions and OH-addition channels versus 1000/T are depicted in Fig. 7. We can clearly see that H-abstraction reactions exhibit obviously negative temperature dependence, while OH-addition channels display slightly positive temperature dependence over the whole temperature range (200–400 K). The total rate constant of H-abstraction channels is 1.17×10^{-12} cm^3 $molecule^{-1}$ s^{-1} at 298 K and 760 Torr, which is two orders of magnitude higher than that of OH-addition pathways (1.08×10^{-14} cm^3 $molecule^{-1}$ s^{-1}) under the same condition. Fig. 7 obviously shows that H-abstraction reactions govern the hydroxylation of DMP. The Arrhenius equations of addition and abstraction reactions over the temperature of 200–400 K are $k_{add} = 5.87 \times 10^{-13}$ exp(−1194/T) and $k_{abs} = 1.82 \times 10^{-13}$ exp(496/T), respectively. In addition, by fitting the whole rate constants in different temperatures, an two-parameter equation ($k = 1.98 \times 10^{-13}$ exp(478/T)) is obtained. Under the pressure of 760 Torr and at 298 K, the overall rate coefficient is 1.18×10^{-12} cm^3 $molecule^{-1}$ s^{-1}.

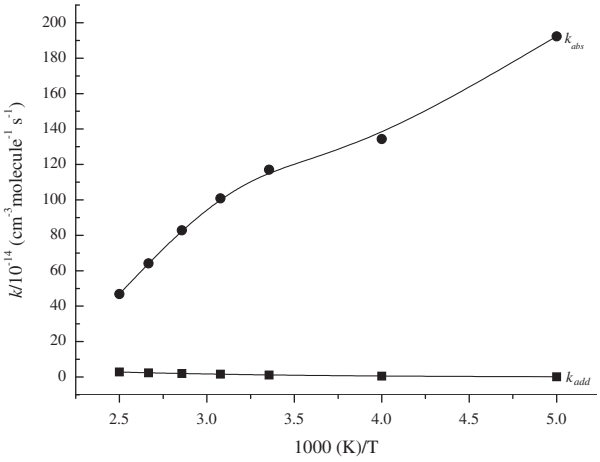

Fig. 7. Branching ratios for the total H-abstraction channels (k_{abs}) and OH-addition channels (k_{add}) at different temperatures.

The individual and whole reaction rate coefficients of DMP + OH over the pressure range of 100–1500 Torr at 298 K are listed in Table 2. Over the whole pressure range, the rate constants are almost the same, about 1.00×10^{-12} cm^3 $molecule^{-1}$ s^{-1}. Rate coefficients are independent of pressure in the studied pressure range. For the reaction of DMP with OH, the half life $t_{1/2}$ is the reciprocal of k[OH], i.e., $t_{1/2} = \frac{\ln 2}{k[OH]}$. Here, k is the total rate constant of the title reaction and [OH] (with the value about 2.0×10^6 molecule cm^{-3})

Table 2
The individual rate constants (cm^{-3} $molecule^{-1}$ s^{-1}) of the primary reaction of DMP + OH at different pressures (Torr).

	100 Torr	300 Torr	700 Torr	740 Torr	760 Torr	800 Torr	1000 Torr	1500 Torr
k_{R1}	2.40E−10	3.41E−09	6.12E−07	4.67E−11	1.06E−10	3.37E−11	2.19E−11	2.08E−11
k_{R1b}	5.53E−09	5.45E−09	6.64E−09	5.98E−09	3.96E−09	5.17E−09	6.61E−09	8.26E−28
k_{R2}	5.25E−09	5.25E−09	5.26E−09	5.25E−09	5.25E−09	5.25E−09	5.25E−09	5.26E−09
k_{R2b}	1.02E−08	1.02E−08	1.03E−08	1.03E−08	5.14E−09	1.03E−08	1.03E−08	1.03E−08
k_{R3}	4.99E−09	5.00E−09	5.00E−09	5.00E−09	3.35E−09	5.00E−09	5.00E−09	5.00E−09
k_{R3b}	8.78E−09	8.78E−09	8.79E−09	8.79E−09	3.84E−09	8.78E−09	8.79E−09	8.80E−09
k_{R4}	1.25E−12	2.32E−12	3.56E−12	3.65E−12	3.70E−12	3.79E−12	4.19E−12	4.98E−12
k_{R4b}	3.02E−12	6.79E−12	1.23E−11	1.28E−11	1.30E−11	1.35E−11	1.56E−11	2.04E−11
k_{R5}	2.36E−12	5.16E−12	9.13E−12	9.47E−12	9.63E−12	9.96E−12	1.15E−11	1.48E−11
k_{R5b}	3.91E−12	8.15E−12	1.38E−11	1.43E−11	1.45E−11	1.49E−11	1.70E−11	2.14E−11
k_{R6}	1.13E−06	1.25E−06	1.30E−06	1.30E−06	1.30E−06	1.30E−06	1.31E−06	1.32E−06
k_{R6b}	6.49E−07	8.68E−07	1.02E−06	1.03E−06	1.04E−06	1.05E−06	1.08E−06	1.14E−06
k	9.07E−13	1.08E−12	1.49E−12	1.18E−12	1.18E−12	1.19E−12	1.22E−12	1.25E−12

(Atkinson and Arey, 2003) is 12-h daylight hydroxyl radical concentration. With respect to degradation with OH, the half life of the DMP at 298 K and 760 Torr is calculated to be 6.8 days in the troposphere.

Due to the lack of corresponding experimental data for comparison, AOP module of EPI Suit package (http://www.epa.gov/opptintr/exposure/pubs/episuitedl.htm) was used for estimating rate constants of the reaction of DMP and OH radical. By applying the same OH concentration and 12 h day, the estimated rate coefficient is 0.57×10^{-12} cm^3 molecule^{-1} s^{-1} and the half life is 14.0 days under 298 K and 760 Torr. The calculated results obtained by performing MESMER program are in agreement with estimated data according to AOP.

4. Conclusions

In this paper, DMP has been selected as a model compound for investigating the oxidation degradation of PAEs in atmosphere using quantum chemical methods. Reaction rate constants are computed using MESMER program. The conclusions are drawn as follows:

(1) Two types of reactions (OH additions to DMP and the hydrogen abstractions) were observed. The calculated results show that abstraction reaction is more likely to occur than hydroxyl addition reaction. Among all the reactions, the hydroxyl radical addition to the *ortho*-carbon of aromatic ring and the H-abstraction from the methyl groups are the most favorable reaction pathways.
(2) IM2 and IM6 are selected to describe their further reaction processes. They will react with NO and O_2. The products of the title reaction are P2-1b-1 ((8*S*)-dimethyl 8-hydroxy-4-oxo-6,7-dioxabicyclo[3.2.1]oct-2-ene-1,2-dicarboxylate), IM6-HNO2 (formic 2-(methoxycarbonyl)benzoic anhydride), oxalaldehyde and several poly-ketones.
(3) The calculated rate constants indicate that OH radicals are likely to react with DMP through abstraction reaction at room temperature and 760 Torr. The total rate constant of addition reactions shows weak positive temperature dependence in discussed temperature ranges, while that of abstraction reactions has negative temperature dependence over the same temperature range. At 298 K and 760 Torr, the total rate constant of the title reaction is 1.18×10^{-12} cm^3 molecule^{-1} s^{-1}. The atmospheric half life of DMP with the respect of OH is estimated to be 6.8 days.

Acknowledgements

This work was supported financially by the National Natural Science Foundation of China (NSFC Nos. 21077067 and 21073220). We thank Dr. Struan H. Robertson for providing the MESMER program.

Appendix A. Supplementary material

Supplementary data associated with this article can be found, in the online version, at http://dx.doi.org/10.1016/j.chemosphere.2013.07.087.

References

Allsopp, M., Santillo, D., Johnston, P., 1997. Poisoning the Future: Impacts of Endocrine-Disrupting Chemicals on Wildlife and Human Health. Greenpeace International, The Netherlands.
Atkinson, R., Arey, J., 2003. Atmospheric degradation of volatile organic compounds. Chem. Rev. 103, 4605–4638.
Douglas, G.R., Hugenholtz, A.P., Blakey, D.H., 1986. Genetic toxicology of phthalate esters: mutagenic and other genotoxic effects. Environ. Health Perspect. 65, 255–262.
Frisch, M.J., Trucks, G.W., Schlegel, H.B., Gill, P.W.M., Johnson, B.G., Robb, M.A., Cheeseman, J.R., Keith, T.A., Petersson, G.A., Montgomery, J.A., Raghavachari, K., Allaham, M.A., Zakrzewski, V.G., Ortiz, J.V., Foresman, J.B., Cioslowski, J., Stefanov, B.B., Nanayakkara, A., Challacombe, M., Peng, C.Y., Ayala, P.Y., Chen, W., Wong, M.W., Andres, J.L., Replogle, E.S., Gomperts, R., Martin, R.L., Fox, D.J., Binkley, J.S., Defrees, D.J., Baker, J., Stewart, J.P., Head-Gordon, M., Gonzales, C., Pople, J.A., 2003. Gaussian 03. Gaussian Inc, Wallingford, CT.
Gonzalez, C., Schlegel, H.B., 1989. An improved algorithm for reaction path following. J. Chem. Phys. 90, 2154–2161.
Güsten, H., Medven, Ž., Sekušak, S., Sabljić, A., 1995. Predicting tropospheric degradation of chemicals: from estimation to computation. SAR QSAR Environ. Res. 4, 197–209.
Harris, C.A., Henttu, P., Parker, M.G., Sumpter, J.P., 1997. The estrogenic activity of phthalate esters in vitro. Environ. Health Perspect. 105, 802–811.
Jobling, S., Reynolds, T., White, R., Parker, M.G., Sumpter, J.P., 1995. A variety of environmentally persistent chemicals, including some phthalate plasticizers, are weakly estrogenic. Environ. Health Perspect. 103, 582–587.
Kovacevic, G., Sabljic, A., 2013a. Theoretical study on the mechanism and kinetics of addition of hydroxyl radicals to fluorobenzene. J. Comput. Chem. 34, 646–655.
Kovacevic, G., Sabljic, A., 2013b. Mechanisms and reaction-path dynamics of hydroxyl radical reactions with aromatic hydrocarbons: the case of chlorobenzene. Chemosphere 92, 851–856.
Lottrup, G., Andersson, A.M., Leffers, H., Mortensen, G.K., Toppari, J., Skakkebaek, N.E., Main, K.M., 2006. Possible impact of phthalates on infant reproductive health. Int. J. Androl. 29, 172–180.
Lynch, B.J., Fast, P.L., Harris, M., Truhlar, D.G., 2000. Adiabatic connection for kinetics. J. Phys. Chem. A 104, 4811–4815.
Main, K.M., Mortensen, G.K., Kaleva, M.M., Boisen, K.A., Damgaard, I.N., Chellakooty, M., Skakkebæk, N.E., 2006. Human breast milk contamination with phthalates and alterations of endogenous reproductive hormones in infants 3 months of age. Environ. Health Perspect. 114, 270–276.
Martell, J.M., Boyd, R.J., 1995. Ab initio studies of reactions of hydroxyl radicals with fluorinated ethanes. J. Chem. Phys. 99, 13402–13411.
Miller, J.A., Klippenstein, S.J., 2006. Master equation methods in gas phase chemical kinetics. J. Phys. Chem. A 110, 10528–10544.
Montuori, P., Jover, E., Morgantini, M., Bayona, J.M., Triassi, M., 2008. Assessing human exposure to phthalic acid and phthalate esters from mineral water stored in polyethylene terephthalate and glass bottles. Food Addit. Contam. 25, 511–518.
Robertson, S.H., Glowacki, D.R., Liang, C.H., Morley, C., Pilling, M.J., 2008. MESMER (Master Equation Solver for Multi-Energy Well Reactions), an object oriented C++ program for carrying out ME calculations and eigenvalue-eigenvector analysis on arbitrary multiple well systems. <http://www.lsourceforge.net/projects/mesmer>.
Sabljić, A., Peijnenburg, W., 2001. Modeling lifetime and degradability of organic compounds in air, soil, and water systems (IUPAC Technical Report). Pure Appl. Chem. 73, 1331–1348.
Sekušak, S., Güsten, H., Sabljić, A., 1995. An ab initio investigation on transition states and reactivity of chloroethane with OH radical. J. Chem. Phys. 102, 7504–7518.
Sekušak, S., Güsten, H., Sabljić, A., 1996. An ab initio study on reactivity of fluoroethane with hydroxyl radical: application of G2 theory. J. Phys. Chem. 100, 6212–6224.
Sekušak, S., Liedl, K.R., Rode, B.M., Sabljić, A., 1997. Reaction-path dynamics of hydroxyl radical reactions with ethane and haloethanes. J. Phys. Chem. A 101, 4245–4253.
Sekušak, S., Sabljić, A., 1997. The role of complexes in hydrogen abstraction from haloethanes by the hydroxyl radical. A case of guided reactions. Chem. Phys. Lett. 272, 353–360.
Staples, C.A., Peterson, D.R., Parkarton, T.F., Adams, W.J., 1997. The environmental fate of phthalate esters: a literature review. Chemosphere 35, 667–749.
Staples, C.A., Parkerton, T.F., Peterson, D.R., 2000. A risk assessment of selected phthalate esters in North American and Western European surface waters. Chemosphere 40, 885–891.
Staples, C.A., Guinn, R., Kramarz, K., Lampi, M., 2011. Assessing the chronic aquatic toxicity of phthalate ester plasticizers. Hum. Ecol. Risk Assess. 17, 1057–1076.
Swan, S.H., Main, K.M., Liu, F., Stewart, S.L., Kruse, R.L., Calafat, A.M., Teague, J.L., 2005. Decrease in anogenital distance among male infants with prenatal phthalate exposure. Environ. Health Perspect. 113, 1056–1061.
Teil, M.J., Blanchard, M., Chevreuil, M., 2006. Atmospheric fate of phthalate esters in an urban area (Paris-France). Sci. Total Environ. 354, 212–223.
US EPA, 1992. Code of federal regulation 40 CFR Part 136.
Vitali, M., Guidotti, M., Macilenti, G., Cremisini, C., 1997. Phthalate esters in freshwaters as markers of contamination sources-a site study in Italy. Environ. Int. 23, 337–347.
Wang, J.L., Liu, P., Qian, Y., 1995. Microbial degradation of di-n-butyl phthalate. Chemosphere 31, 4051–4056.
Wang, P., Wang, S.L., Fan, C.Q., 2008. Atmospheric distribution of particulate- and gas-phase phthalic esters (PAEs) in a Metropolitan City, Nanjing, East China. Chemosphere 72, 1567–1572.